Cell Death and Differentiation (2004) 11, 1166–1178
© 2004 Nature Publishing Group All rights reserved 1350-9047/04 $30.00
www.nature.com/cdd

Irradiation-induced progenitor cell death in the developing brain is resistant to erythropoietin treatment and caspase inhibition

H Fukuda[1,2], A Fukuda[1,2], C Zhu[1,3], L Korhonen[4], J Swanpalmer[5], S Hertzman[5], M Leist[6], B Lannering[7], D Lindholm[4], T Björk-Eriksson[8], I Marky[7] and K Blomgren*[,1,7]

[1] Perinatal Center, Department of Physiology, Göteborg University, Box 432, SE 405 30 Göteborg, Sweden
[2] Department of Obstetrics and Gynecology, Osaka University School of Medicine, 2-2 Yamada-oka, Suita 565-0871, Japan
[3] Department of Pediatrics, The Third Affiliated Hospital of Zhengzhou University, 450052 Zhengzhou, PR China
[4] Department of Neuroscience, Uppsala University, BMC Box 587, SE 75123 Uppsala, Sweden
[5] Department of Radiation Physics, Sahlgrenska University Hospital, SE 413 45 Göteborg, Sweden
[6] Molecular Disease Biology, H Lundbeck A/S, Ottiliavej 9, DK 2500 Valby, Denmark
[7] Department of Pediatrics, The Queen Silvia Children's Hospital, SE 416 85 Göteborg, Sweden
[8] Department of Oncology, Sahlgrenska University Hospital, SE 413 45 Göteborg, Sweden
* Corresponding author: K Blomgren, Perinatal Center, Department of Physiology, Göteborg University, Box 432, SE 405 30 Göteborg, Sweden. Tel: +46 31 773 3376; Fax: +46 31 773 3512; E-mail: klas.blomgren@fysiologi.gu.se

Received 17.12.03; revised 15.4.04; accepted 29.4.04; published online 09.7.04
Edited by V De Laurenzi

Abstract

One hemisphere of postnatal day 8 (P8) rats or P10 mice was irradiated with a single dose of 4–12 Gy, and animals were killed from 2 h to 8 weeks after irradiation (IR). In the subventricular zone (SVZ) and the granular cell layer (GCL) of the dentate gyrus, harboring neural and other progenitor cells, nitrosylation and p53 peaked 2–12 h after IR, followed by markers for active caspase-3, apoptosis-inducing factor and TUNEL (6–24 h). Ki67-positive (proliferating) cells had disappeared by 12 h and partly reappeared by 7 days post-IR. The SVZ and GCL areas decreased approximately 50% 7 days after IR. The development of white matter was hampered, resulting in 50–70% less myelin basic protein staining. Pretreatment with erythropoietin did not confer protection against IR. Caspase inhibition by overexpression of XIAP prevented caspase-9 and caspase-3 activation but not cell death, presumably because of increased caspase-independent cell death.

Cell Death and Differentiation (2004) **11,** 1166–1178.
doi:10.1038/sj.cdd.4401472
Published online 9 July 2004

Keywords: irradiation; developing brain; apoptosis; caspase; AIF; nitrotyrosine; neurogenesis; subventricular zone; subgranular zone

Abbreviations: AIF, apoptosis-inducing factor; DG, dentate gyrus; Epo, erythropoietin; GCL, granular cell layer (dentate gyrus of the hippocampus); HI, hypoxia–ischemia; IAP, inhibitor of apoptosis protein; IOD, integrated optical density; IR, irradiation; MBP, myelin basic protein; P8, postnatal day 8; P10, postnatal day 10; PBS, phosphate-buffered saline; RT, radiation therapy; SGZ, subgranular zone (in the dentate gyrus of the hippocampus); SVZ, subventricular zone; TBS-T, Tris-buffered saline with 0.1% Tween 20; TG-XIAP, transgenic XIAP overexpression; WT, wild type; XIAP, X-linked inhibitor of apoptosis protein

Introduction

Radiation therapy (RT) is one of the most effective tools in the treatment of malignant tumors, and is applied not only to adult patients but also to children who suffer from primary or metastatic brain tumors and central nervous system involvement of leukemia and lymphoma. It is reported that 75% of all children struck with cancer are cured using a combination of RT and other therapies.[1] However, the tough therapy has both acute and long-lasting, severe side effects. Even low doses of ionizing radiation to the brain can cause intellectual impairment as well as perturbed growth and puberty.[2–6] RT can cause vascular abnormalities, demyelination and ultimately necrosis.[7] These problems are more pronounced for children who receive RT and the intensity of symptoms seems to be correlated with the age of the child at the time of treatment, such that the younger the child at the time of RT the more severe the symptoms.[8] Up to half of the children who received cranial RT developed significant intellectual or behavioral retardation, and these symptoms were more severe in children less than 3 years of age at the time of RT.[8–11] In addition to these neuropsychological complications, short stature resulting from growth hormone secretory or regulatory dysfunction has also been reported in the majority of brain tumor patients who received RT.[4,12–14] If the severe aftereffects of the anticancer therapy can be reduced, the overall quality of life would be greatly improved for the increasing number of children who survive their cancer.

Ionizing radiation can cause DNA damage either directly through ionization of the DNA, or indirectly through the generation of free radicals. Highly proliferating cells tend to undergo apoptosis after IR, whereas other cells may enter a stage of growth arrest and DNA repair. Neurons can be considered to be in a permanent stage of growth arrest, but the regions containing stem cells and progenitor cells, such as the hippocampal subgranular zone (SGZ) of the dentate gyrus (DG) and the subventricular zone (SVZ), have a high proliferation capacity. Postnatal neurogenesis probably plays an important role in normal hippocampal function,[15–17] and IR has been demonstrated to decrease neuronal

proliferation[18,19] and contribute to memory dysfunction in rodents.[20,21] Malignant cells are generally highly sensitive to IR because of their loss of growth regulation and genomic stability. However, as part of the perturbed growth regulation, most tumor cells have lost their ability to undergo apoptosis, which means that they will die through mitotic catastrophe or senescence-like permanent growth arrest upon RT.[22] Hence, provided that the molecular mechanisms can be characterized, an antiapoptotic strategy may prove successful in protecting the normal tissue, still allowing IR to eliminate tumor cells.

In this study, we have set up and characterized a rodent model of acute RT injury to the developing brain, using 8-day-old rats and 10-day-old mice. We also examined the effect of antiapoptotic strategies on IR-induced brain injury, using erythropoietin (Epo) treatment or caspase inhibition through neuronal transgenic X-linked inhibitor of apoptosis protein overexpression (TG-XIAP) in mice.

Results

Time course of the acute cellular injury in the GCL

Postnatal day 8 (P8) rats were subjected to unilateral IR, using a single dose of 4, 8 or 12 Gy. Representative photomicrographs of the DG in control animals and in the ipsilateral hemisphere after 8 Gy, stained for p53, nitrotyrosine, active caspase-3, apoptosis-inducing factor (AIF) and TdT-mediated dUTP nick end labeling (TUNEL) are shown in Figure 1. Very few positive cells were detected in control brains, but all of the five markers of cellular injury appeared within 6 h, predominantly in the SGZ of the DG, but to some extent also in the hilus and the granular cell layer (GCL) (Figure 1). Nitrotyrosine- and p53-positive cells appeared in both hemispheres already 2 h after IR, but the number of positive cells was higher in the ipsilateral hemisphere (Figure 2). From 6 h onwards, there were very few p53-positive cells, but the number of nitrotyrosine-positive cells remained at a high level for at least 12 h after IR. The apoptosis-related markers active caspase-3, AIF and TUNEL all appeared later than nitrotyrosine and p53, displaying a peak around 6–12 h post-IR in the GCL (Figure 2). The apoptosis-related markers appeared also in the contralateral nonirradiated hemisphere, typically 20–50% fewer than in the ipsilateral GCL (Figure 2). At early recovery (2 h), most cells positive for the injury markers displayed an irregular shape, but at 6 and 12 h after IR, most of the stained cells appeared pyknotic, being uniformly round, small, densely stained and displaying compact nuclei. These positive cells disappeared 24 h after IR, indicating that they

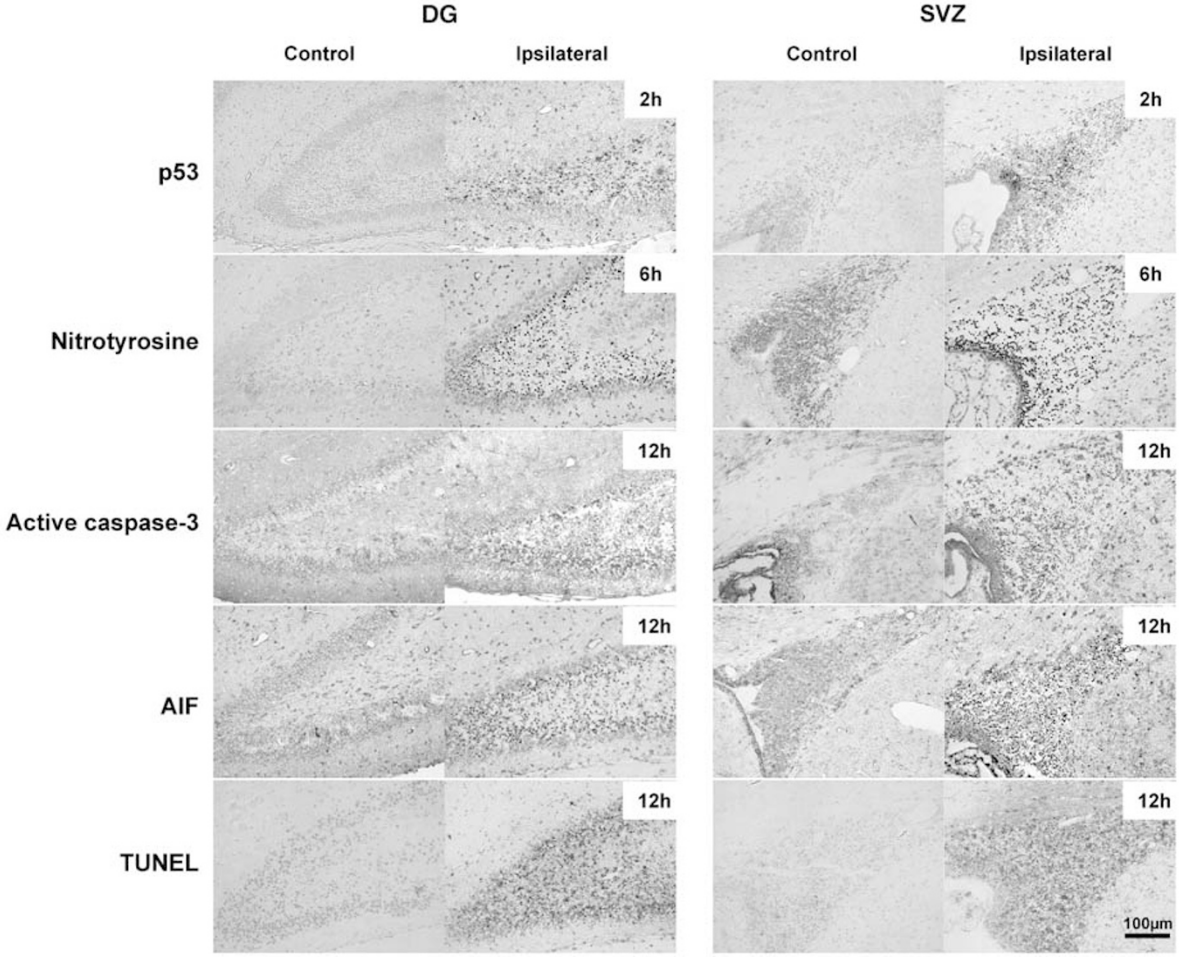

Figure 1 Representative microphotographs of the DG (left panel) and the SVZ (right panel) in nonirradiated control animals and at one specific time point after IR (2, 6 or 12 h), demonstrating the staining of p53, nitrotyrosine (a marker of oxidative stress), active caspase-3, AIF and TUNEL (a marker of DNA damage). Scale bar: 100 μm

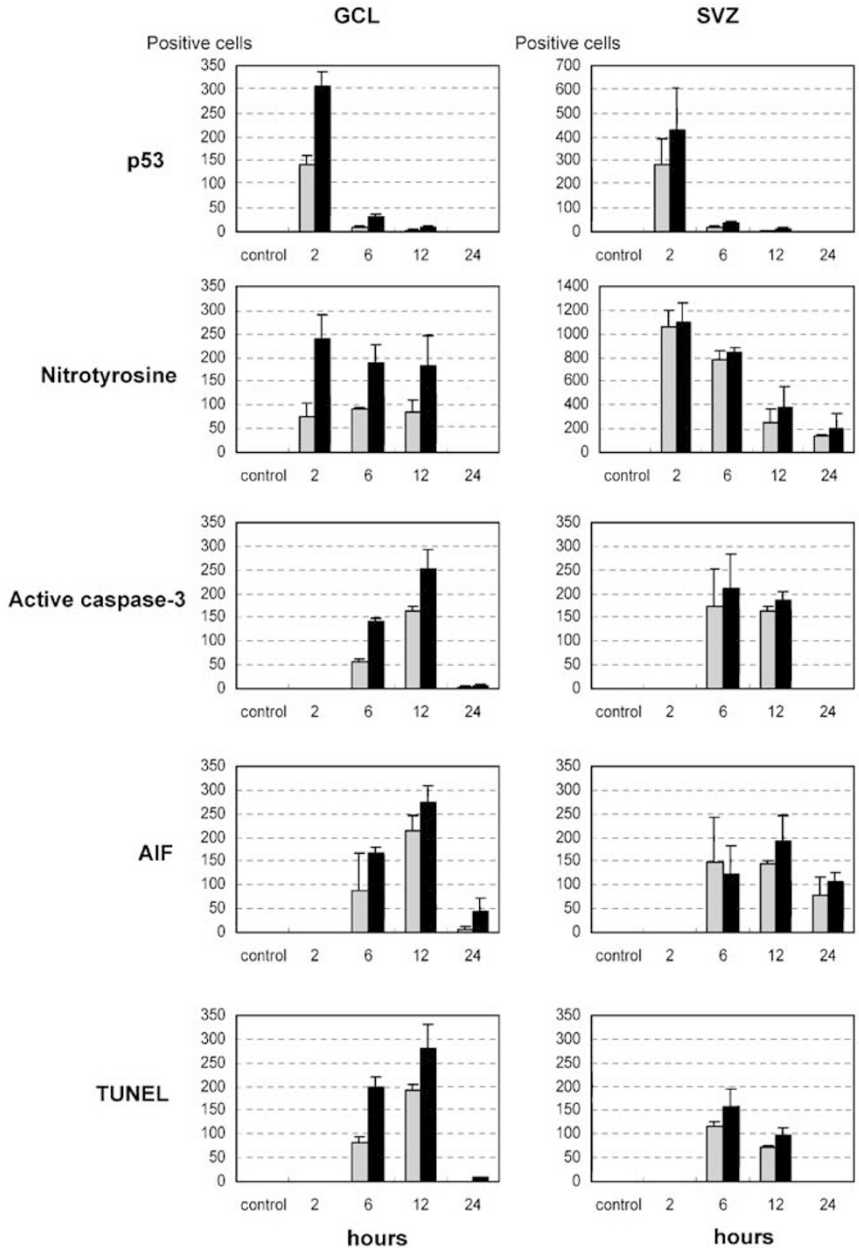

Figure 2 Time course of the appearance and clearance of cellular injury markers in the GCL (left column) of the DG and in the SVZ (right column), as in Figure 1, from nonirradiated control animals (control) and 2, 6, 12 and 24 h after 8 Gy IR. Counting of positive cells was performed as described in Materials and methods and expressed as average $\pm$ S.D. in control animals (white bars), the contralateral hemispheres (gray bars) and the ipsilateral hemispheres (black bars)

had been cleared by phagocytes or autophagy. The AIF-positive cells were considerably smaller than the active caspase-3-positive cells (not shown), indicating either that they are different populations of cells or different stages of cell death. In control sections, cells in the SGZ displayed weak AIF immunoreactivity, but 12 h after 8 Gy IR, nuclear AIF immunoreactivity was strong in some cells, and these cells displayed pyknotic, fragmented nuclei (Figure 3a). Translocation from an exclusively non-nuclear to a partially nuclear immunoreactivity of AIF was evident in numerous cells after IR (Figure 3b), as demonstrated earlier in neurons after adult[23] and neonatal ischemia.[24]

Time course of the acute cellular injury in the SVZ

In the SVZ, the staining patterns were similar to the GCL, but there were also obvious differences (Figure 1). Generally, the numbers of positive cells in the ipsi- and contralateral hemispheres were quite similar in the SVZ, much more so than in the GCL (Figure 2). Nitrotyrosine-positive cells were

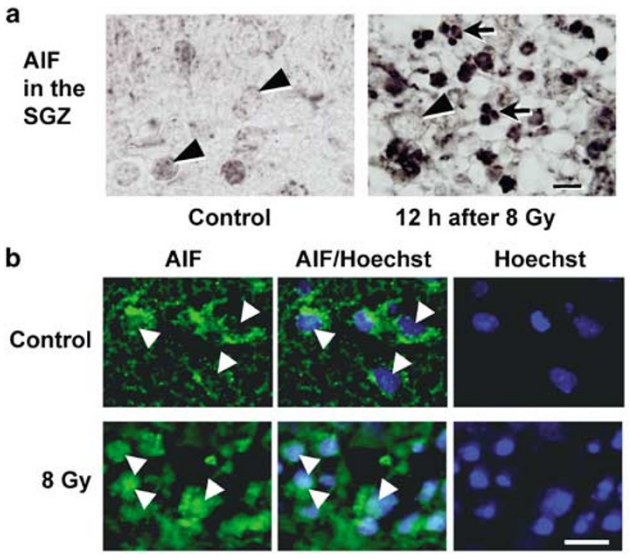

Figure 3 Two figures showing nuclear translocation of AIF immunoreactivity after IR in the SGZ of the DG in the hippocampus. (**a**) Bright or gray AIF immunoreactivity in the normal cells (arrowheads) of the nonirradiated SGZ (left panel), but 12 h after IR numerous cells in this region displayed pyknotic, fragmented nuclei with dense, black AIF immunoreactivity (long arrows) (right panel). (**b**) AIF immunoreactivity (green) combined with the nuclear stain Hoechst 3342 (blue), demonstrating that AIF immunoreactivity is exclusively non-nuclear in normal, nonirradiated cells (arrows), whereas after IR much of the AIF immunoreactivity, but not all, was colocalized with the nuclear stain (arrows). Scale bar in (**a**, **b**): 10 μm

present mainly 2 h post-IR, more pronounced in the medial SVZ, near the ventricles (Figure 1) and disappeared at a different rate than in the GCL (Figure 2). The peak of caspase-3- and AIF-positive cells appeared somewhat earlier in the SVZ than in the GCL (Figure 2).

Effect of irradiation on proliferating cells

The number of Ki-67-positive cells in control animals was about the same at P8 (Figure 4a) and P15 (Figure 4b) in the GCL (Figure 4c) and in the SVZ (Figure 4d). In irradiated animals, the number of positive cells was unchanged 2 h after IR (Figure 4c and d). At 12 h after the insult, the Ki-67-positive cells had disappeared from the ipsilateral hemisphere (Figure 4a, c and d) and decreased to about 20 and 10% in the contralateral hemispheres of the GCL (Figure 4c) and the SVZ (Figure 4d), respectively. The Ki-67-positive cells reappeared to a certain extent after 24 h and 7 days recovery, more pronounced in the SVZ (Figure 4c and d).

Assessment of injury

GCL and SVZ areas

There was a dose-dependent reduction of the size of both the GCL (Figure 5a) and the SVZ (Figure 5b) in the ipsilateral hemisphere 7 days after IR. The average GCL area in a control animal was $0.31 \pm 0.03\,mm^2$ (Figure 5c). The GCL area in the ipsilateral, irradiated hemisphere was significantly decreased 7 days after IR, to 70, 50 and 48% of the control

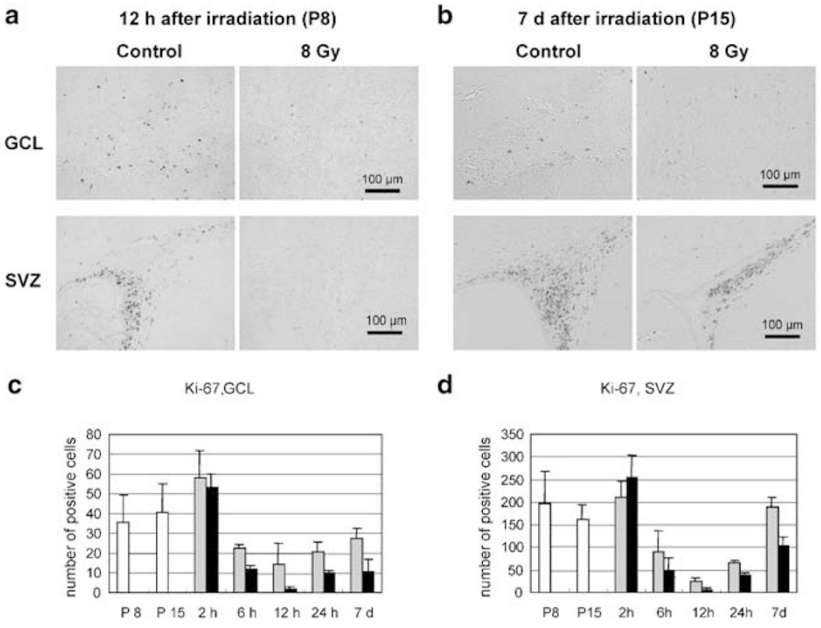

Figure 4 Staining for Ki-67, a marker of proliferating cells. (**a**) Representative stainings of the GCL and SVZ in control animals (P8) and 12 h after 8 Gy IR, demonstrating a basal level of proliferating cells in these areas, more pronounced in the SVZ, in control animals, and that these cells virtually disappear 12 h after IR. (**b**) Representative stainings of the GCL and SVZ in control animals (P15) and 7 days after 8 Gy IR, demonstrating that the basal level of proliferation is the same as at P8, and that a partial recovery has occurred 7 days after 8 Gy IR, more so in the SVZ than in the GCL. (**c**) Quantification of the number of Ki-67-positive cells, as described in Materials and methods, in the GCL of control animals (P8 and P15) and from 2 h to 7 days after IR in the contralateral (gray) and ipsilateral (black) hemispheres. Average $\pm$ S.D. (**d**) Quantification of the number of Ki-67-positive cells, as described in Materials and methods, in the SVZ of control animals (P8 and P15) and from 2 h to 7 days after IR in the contralateral (gray) and ipsilateral (black) hemispheres. Average $\pm$ S.D.

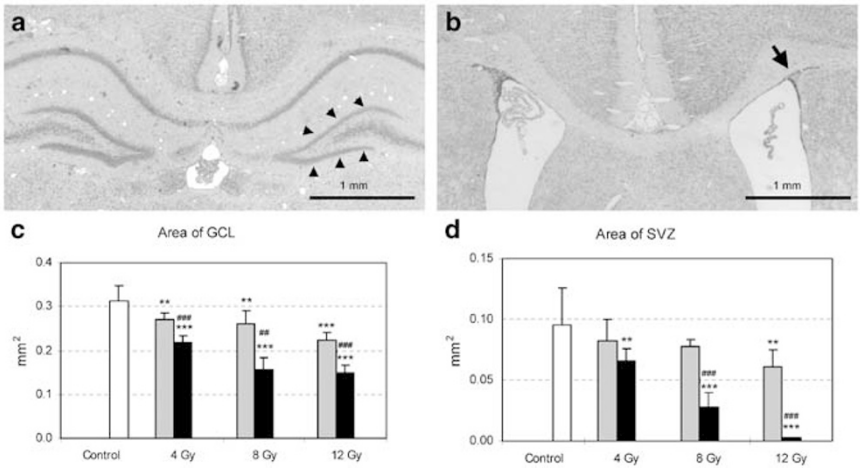

Figure 5 Representative microphotographs of the GCL in the DG (**a**) and the SVZ (**b**) 7 days after 8 Gy IR, demonstrating a decreased area of these regions. (**c**) The average GCL area in control animals (white bars), the contralateral hemispheres (gray bars) and the ipsilateral hemispheres (black bars) 7 days after 4, 8 or 12 Gy IR. The GCL was manually traced in three equally spaced sections per animal and six animals per dose were evaluated. (**d**) The average SVZ area in control animals (white bars), the contralateral hemispheres (gray bars) and the ipsilateral hemispheres (black bars) 7 days after 4, 8 or 12 Gy IR. The SVZ was manually traced in three equally spaced sections per animal and six animals per dose were evaluated. $^{**}P<0.01$ and $^{***}P<0.001$ using ANOVA and Fischer's PLSD *post hoc* test, comparing the irradiated hemispheres with the controls. $\#\#P<0.01$ and $\#\#\#P<0.001$ using Student's *t*-test comparing the ipsi- and contralateral hemispheres after the same IR dose

animals after 4, 8 and 12 Gy, respectively (Figure 5c). The GCL area in the contralateral, nonirradiated hemisphere was also significantly decreased 7 days after IR, to 87, 74 and 71% of the control animals after 4, 8 and 12 Gy, respectively (Figure 5c). Comparing the two hemispheres in the same animal, the ipsilateral GCL was significantly smaller than the contralateral GCL after all the three IR doses tried (Figure 5c). The average SVZ area in a control animal was $0.10 \pm 0.03\,mm^2$ (Figure 5d). The SVZ area in the ipsilateral, irradiated hemisphere was significantly decreased 7 days after IR, to 67, 30 and 2.5% of the control animals after 4, 8 and 12 Gy, respectively (Figure 5d). The SVZ area in the contralateral, nonirradiated hemisphere was also affected 7 days after IR, being 87, 82 and 64% of the control animals after 4, 8 and 12 Gy, respectively (Figure 5d), statistically significant after 8 and 12 Gy. Within the same brain, the ipsilateral SVZ was significantly smaller than the contralateral SVZ 7 days after 8 and 12 Gy, but not after 4 Gy (Figure 5d).

Myelination

Representative microphotographs of myelin basic protein (MBP) stainings at the striatum level 7 days after 8 Gy are shown in Figure 5a. The integrated optical density (IOD) of the MBP staining was evaluated separately in the corpus callosum and cortex (CC&C) on the one hand and in the striatum (Stri) on the other. The average IOD of the MBP-positive areas in the CC&C in one hemisphere from a control animal was 1.45 ± 0.14 arbitrary units (Figure 6b). This decreased significantly in the ipsilateral hemisphere, to 58, 41 and 41% of the IOD in the control animals, after 4, 8 and 12 Gy, respectively (Figure 6b). In the contralateral, non-irradiated hemisphere, the MBP staining in the CC&C was also decreased, to 90, 86 and 74% of control animals after 4, 8 and 12 Gy, respectively, but statistically significant only after 8 and 12 Gy (Figure 6b). The myelination in the striatum was even more affected in the ipsilateral hemisphere. In the control animals, the MBP IOD was 0.58 ± 0.08 (Figure 6c). This decreased significantly in the ipsilateral hemisphere, to 58, 15 and 26% of the IOD in the control animals, after 4, 8 and 12 Gy, respectively (Figure 6c). In the contralateral striatum, the MBP staining decreased, to 90, 75 and 72% of control animals after 4, 8 and 12 Gy, respectively, statistically significant only after 8 and 12 Gy (Figure 6c).

Body and brain weight

There was no significant difference in the body weights of control animals and those exposed to 8 Gy unilateral or bilateral IR up to 7 days post-IR. However, 4 and 8 weeks after IR, the animals subjected to bilateral IR displayed significantly decreased body weights (34 and 24% after 4 and 8 weeks, respectively), whereas those subjected to unilateral IR did not show any significant differences in body weight (Figure 6). The whole brain weight decreased 12% ($P<0.01$) 8 weeks after unilateral and 21% ($P<0.001$) after bilateral IR (Figure 7).

Dose–response in the activation of p53 and caspase-3

There were no p53-positive cells in the nonirradiated animals, and there was a clear dose–response correlation between the IR dose and the number of cells positive for p53 in the GCL (Figure 8a) and SVZ (Figure 8a) 6 h after IR. There were few p53-positive cells in the contralateral, nonirradiated GCL or SVZ after 4 Gy (5.9 and 19% of the numbers in the ipsilateral hemisphere, respectively) (Figure 8a and b), but after 12 Gy the number of p53-positive cells was similar to the number in the ipsilateral hemisphere (66 and 93% in the GCL and SVZ, respectively) (Figure 8a and b), indicating that the scattered,

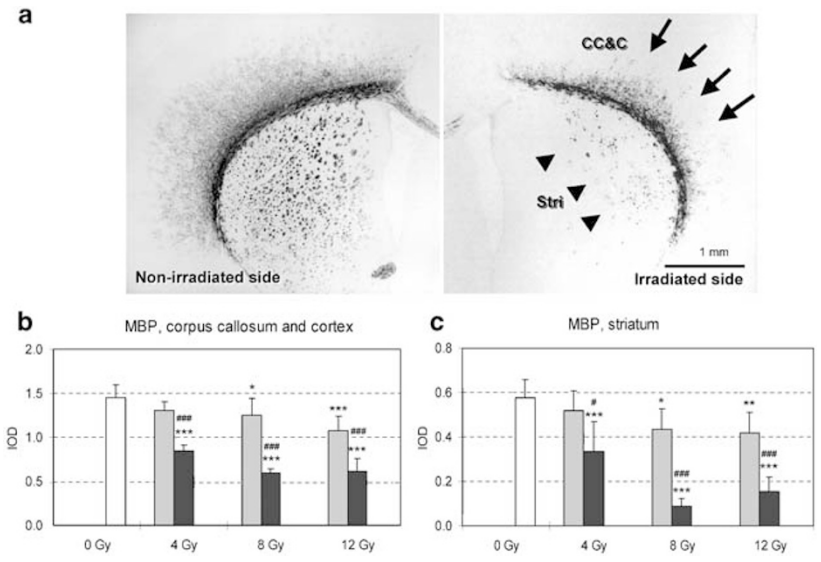

Figure 6 (**a**) Representative microphotographs of MBP staining showing the white matter in the corpus callosum and cortex (CC&C) and the striatum (Stri) in the nonirradiated hemisphere (left panel) and the irradiated hemisphere (right panel) 7 days after 8 Gy. Long arrows indicate the area with decreased MBP staining in the CC&C. The arrowheads indicate the loss of MBP staining in the striatum. (**b**) The average IOD of the MBP staining ± S.D. in the CC&C in control animals (white bars), the contralateral hemispheres (gray bars) and the ipsilateral hemispheres (black bars) 7 days after 4, 8 or 12 Gy IR. The MBP IOD was manually traced in three equally spaced sections per animal and six animals per dose were evaluated. (**c**) The average MBP IOD ± S.D. in the striatum in control animals (white bars), the contralateral hemispheres (gray bars) and the ipsilateral hemispheres (black bars) 7 days after 4, 8 or 12 Gy IR. The SVZ was manually traced in three equally spaced sections per animal and six animals per dose were evaluated. $*P<0.05$, $**P<0.01$ and $***P<0.001$ using ANOVA and Fischer's PLSD *post hoc* test, comparing the irradiated hemispheres with the controls. $\#\#P<0.01$ and $\#\#\#P<0.001$ using Student's *t*-test comparing the ipsi- and contralateral hemispheres after the same IR dose

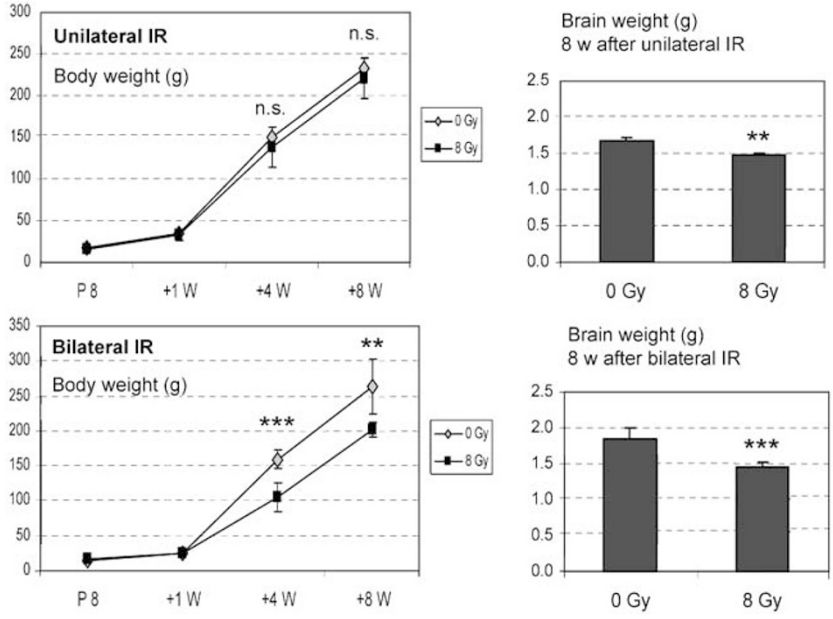

Figure 7 The left panels demonstrate the body weights of nonirradiated rats (gray diamonds) and rats treated with 8 Gy (black squares) at the time of IR (P8) and 1, 4 and 8 weeks after IR. The upper left panel shows the body weights of animals where only one hemisphere was irradiated (unilateral IR) and the lower left panel shows the body weights of animals where both hemispheres were irradiated (bilateral IR). The right panels show the brain weights of animals 8 weeks after 8 Gy unilateral (upper right panel) or bilateral (lower right panel) IR. $n=3$–6 animals per group. $**P<0.01$, $***P<0.001$ and n.s.: nonsignificant using Student's *t*-test to compare nonirradiated and irradiated animals in the same group

secondary IR was substantial after 12 Gy but not after 4 Gy. The dose–response for activation of caspase-3 was similar to that of p53. There were no positive cells in the nonirradiated animals, and there was a considerable increase with increasing IR dose (Figure 8c and d). Interestingly, the activation of caspase-3 in the contralateral, nonirradiated hemisphere was limited in the GCL (11, 9.0 and 45% of the number of caspase-3-positive cells in the ipsilateral hemisphere after 4, 8 and

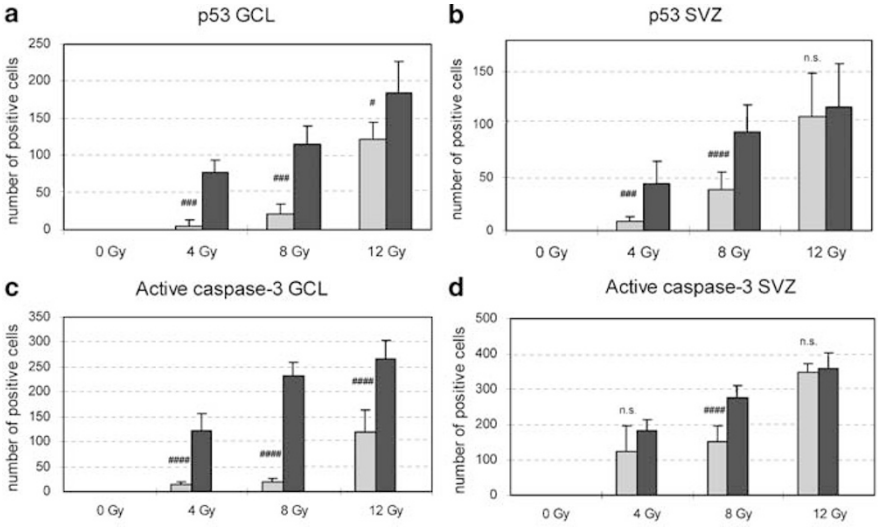

Figure 8 A dose–response is demonstrated between the IR dose and the number of cells positive for p53 (**a**, **b**) and active caspase-3 (**c**, **d**). (**a**) The number of cells positive for p53 in the GCL. (**b**) The number of cells positive for p53 in the SVZ. (**c**) The number of cells positive for active caspase-3 in the GCL. (**d**) The number of cells positive for active caspase-3 in the SVZ. White bars represent control animals, gray bars the contralateral hemispheres and black bars the ipsilateral hemispheres. Counting was performed as described in Materials and methods 6 h after 4, 8 or 12 Gy IR. $n = 6$ animals per group. $^{*}P < 0.05$, $^{**}P < 0.01$, $^{***}P < 0.001$ and n.s.: nonsignificant using Student's *t*-test to compare the ipsi- and contralateral hemispheres after the same IR dose

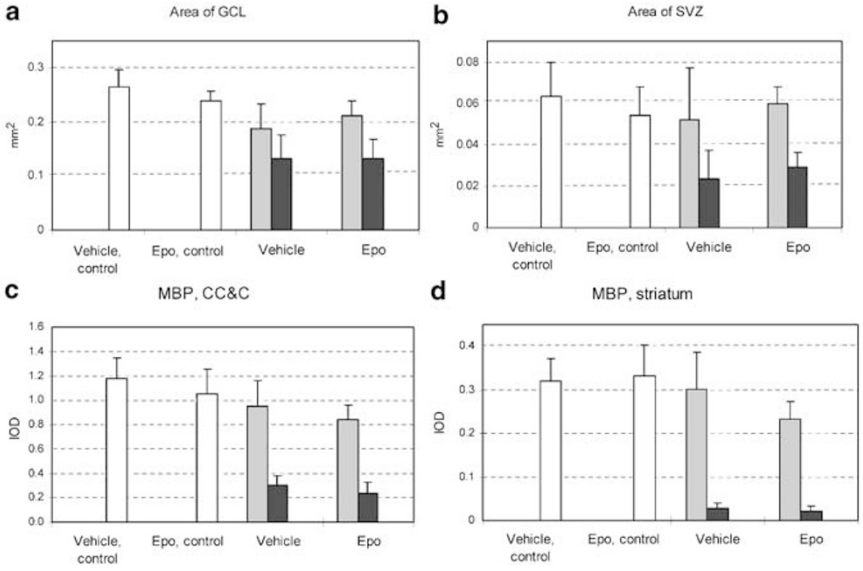

Figure 9 Evaluation of the injury 7 days after 8 Gy IR in Epo-treated and vehicle-treated animals was performed by measuring the area of the GCL (**a**), the area of the SVZ (**b**), the MBP IOD in the corpus callosum and cortex (CC&C) (**c**) and the MBP IOD in the striatum (**d**). White bars indicate nonirradiated control animals, gray bars contralateral hemispheres and black bars ipsilateral hemispheres. The mean $\pm$ S.D. is indicated for the different parameters. No statistically significant differences could be detected between the vehicle- and Epo-treated groups ($n = 10$ animals per group)

12 Gy, respectively), but considerably higher in the SVZ even after a low dose of IR (69, 55 and 97% of the number of caspase-3-positive cells in the ipsilateral hemisphere after 4, 8 and 12 Gy, respectively) (Figure 8c and d).

Effects of erythropoietin

To examine the effects of Epo, 8-day-old rats were treated with a single intraperitoneal dose of recombinant human Epo 4 h prior to IR (8 Gy). The animals were killed 7 days after IR and injury was assessed as described above.

Vehicle- and Epo-treated animals not subjected to IR displayed no significant differences in their GCL or SVZ areas or in their MBP IODs (Figure 9). There were no significant differences between the Epo- and vehicle-treated animals 7 days after IR, neither in the ipsilateral nor in the contralateral hemispheres with respect to any of the four injury parameters measured (Figure 9).

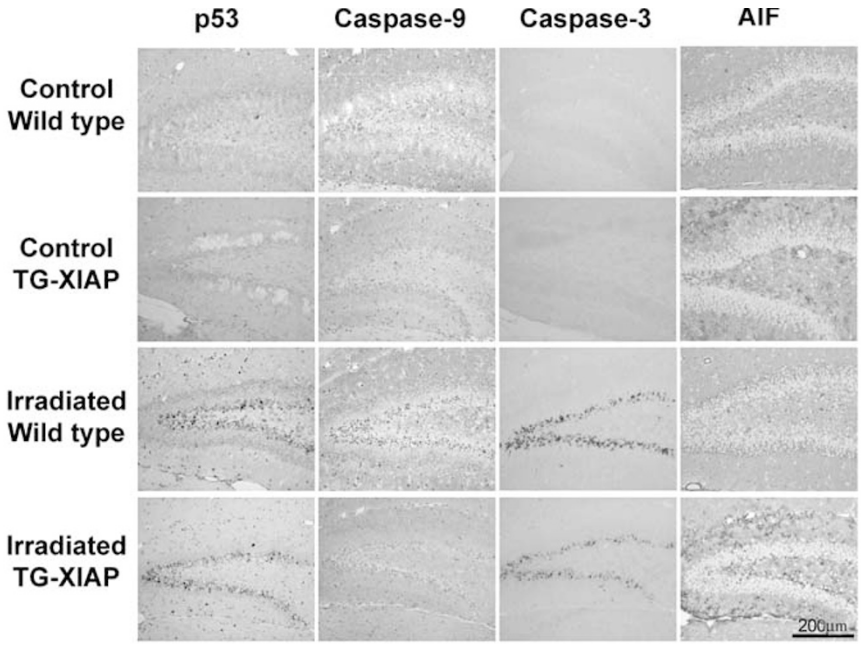

Figure 10 Representative stainings of the ipsilateral DG in the hippocampus, including the GCL and the proliferative SGZ, 6 h after 8 Gy IR. Nonirradiated (control) and irradiated mice, both WT (WT) and XIAP-overexpressing (TG-XIAP) are shown for the four different markers of injury indicated above the microphotographs. Immunopositive cells are mainly found in the proliferative SGZ, the interface between the GCL and the hilus

Effects of XIAP overexpression

Inhibitor of apoptosis (IAP) proteins are endogenous anti-apoptotic proteins capable of inhibiting caspases, and XIAP is the most potent of the IAPs.[25] To examine the effects of caspase inhibition on brain injury, TG-XIAP mice were irradiated unilaterally with 8 Gy and killed 6 h and 7 days after IR. Representative immunostainings of the DG 6 h post-IR are shown in Figure 10. Caspase activation, as judged by the average numbers of cells per DG area positive for active caspase-9 and active caspase-3, was reduced in TG-XIAP mice (211.7 ± 61.2 in wild type (WT) *versus* 49.8 ± 60.5 in TG-XIAP for active caspase-9, $P = 0.0017$, and 212.2 ± 45.0 in WT *versus* 77.0 ± 25.3 in TG-XIAP for active caspase-3, $P = 0.0001$) (Figure 11). The number of AIF-positive cells, on the other hand, was increased (68.0 ± 17.7 in WT *versus* 165.0 ± 79.4 in TG-XIAP, $P = 0.0447$) (Figure 11). The number of p53-positive cells was unchanged (127.0 ± 26.1 *versus* 128.4 ± 33.8, $P = 0.943$) (Figure 11). The ipsilateral GCL areas (including the SGZ) of animals killed 7 days post-IR were significantly reduced compared with the nonirradiated controls (approx. 30%, $P < 0.0001$) (Figure 12a), but the reduction was not significantly different between WT and TG-XIAP mice (Figure 12b).

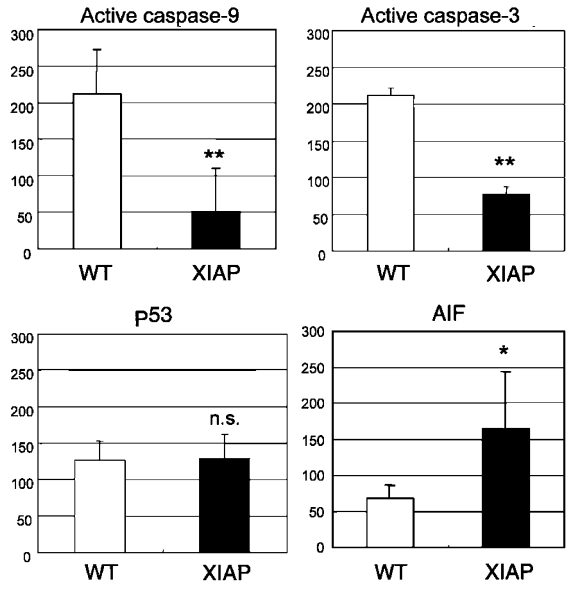

Figure 11 The average number of immunopositive cells in the ipsilateral DG 6 h after 8 Gy is compared between WT (WT) ($n = 6$) and XIAP-overexpressing (XIAP) ($n = 5$) mice, as described in Materials and methods. The bars indicate the average number of positive cells per section $\pm$ S.D. ***$P < 0.001$, **$P < 0.01$, *$P < 0.05$ and n.s.: nonsignificant, using Student's unpaired *t*-test

Discussion

In this study, we have characterized a novel model of radiation-induced injury to the developing brain, and have tested two different, presumably antiapoptotic, strategies to protect the normal brain tissue from the detrimental effects of IR, Epo treatment and inhibition of caspases by means of transgenic overexpression of the inhibitor XIAP. Children with malignant brain tumors often need radiotherapy to be cured. The tumor receives a high total dose (40–55 Gy), but the normal brain tissue may also receive a substantial IR dose. IR to the developing brain causes acute and late side effects, which may seriously impair future neuropsychological

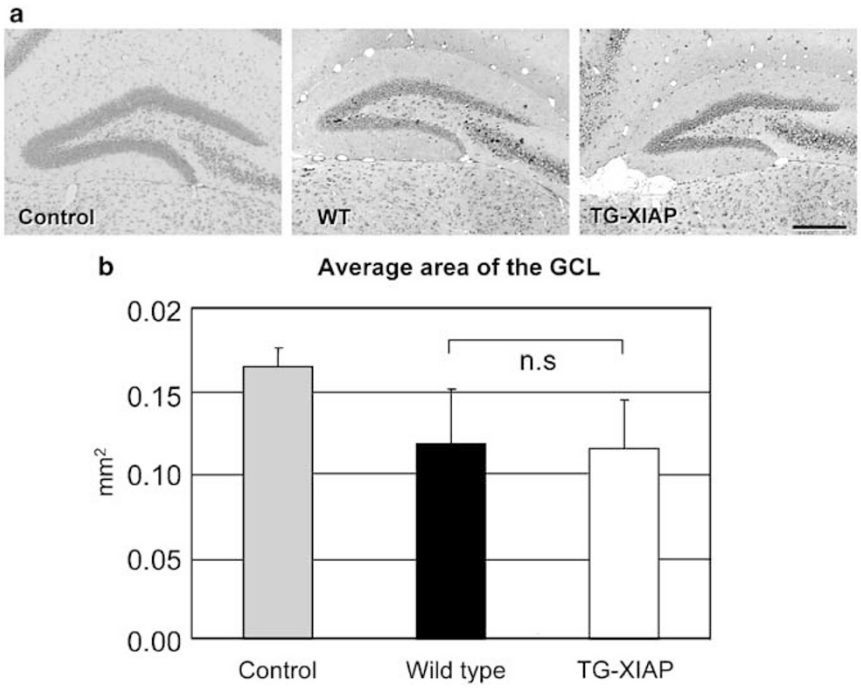

Figure 12 (**a**) Representative stainings of the ipsilateral DG in the hippocampus 7 days after 8 Gy IR, comparing nonirradiated WT (control) with irradiated WT (WT) and XIAP-overexpressing (TG-XIAP) mice. Sections were stained with thionin/acid fuchsin as described in Materials and methods. Scale bar: 200 μm. (**b**) The average area of the DG (GCL + SGZ) per section, measured as described in Materials and methods, 7 days after 8 Gy is compared between nonirradiated animals, and between the ipsilateral hemispheres of WT and XIAP-overexpressing (TG-XIAP) mice. The bars indicate the average area per section $\pm$ S.D. The number of animals used is 15, 12 and 11 for the nonirradiated controls, WT and TG-XIAP, respectively. n.s.: nonsignificant, using ANOVA and Fischer's PLSD

development.[2,26] Using the LQ model[27] and an α/β ratio of 3 for late effects in the normal brain tissue, the acute exposures of 4, 8 and 12 Gy are equivalent to approximately 6, 18 and 43 Gy, respectively, when delivered in repeated 2 Gy fractions. These dose levels represent clinically relevant doses, that is, 10, 30 and 80% isodoses in radical radiotherapy of malignant brain tumors in children. We characterized the time course of the IR-induced injury studying the two main regions in the brain where stem cells and progenitors reside, the SVZ and the SGZ. We also studied the developing white matter, as immature oligodendrocytes are known to be vulnerable to various insults.[28] As judged by the stainings employed, no overt injury could be detected in areas outside the proliferative zones or the immature oligodendrocytes. The irradiated animals displayed hair loss on the ipsilateral side of the skull, but weight gain and behavior were not different from nonirradiated littermates. Using unilateral IR prevented the stunting seen in rats subjected to bilateral IR, at least up to 8 weeks post-treatment, and unilateral IR also reduced the loss of brain weight, consistent with earlier findings.[29,30] This is an advantage especially when allowing long-term survival. The IR is not truly unilateral, because considerable secondary radiation is scattered into the contralateral hemisphere, as judged by the dose-dependent appearance of injury markers.

It has been demonstrated that the cells in the SVZ[31] and the SGZ[32,33] of the adult brain undergo apoptosis following ionizing radiation. Moreover, the size of the SVZ in adult rats reflects the number of proliferating cells, indicating that it is a good marker of SVZ precursor proliferation.[34] Following IR to the adult brain, neurogenesis, but not gliogenesis, in the DG was decreased,[19] and extensive, long-lasting activation of microglia could be demonstrated.[35,36] Monje and co-workers[19] showed that the neural precursor cells in the DG retained, or even increased, their capacity to generate new neurons after IR if cultured *in vitro*, but not when remaining *in situ*, an effect that was at least partly attributed to IL-6 expression.[35] This indicates that IR, apart from inducing overt cell death, also generates a hostile environment for neural precursors. The decreased myelination observed after IR in our paradigm is different from the radionecrosis of white matter observed in the adult brain, which evolves slowly over months. In rats, the proliferation of oligodendroglial cells begins after birth, and is completed approximately around P21. Myelination begins around P10 and accelerates between P16 and P30 with a maximum at P20.[37] The lack of myelination observed in this study is manifested faster than demyelination after radionecrosis, and most likely reflects a loss of pre-oligodendrocytes and immature oligodendrocytes. Immature oligodendrocytes are known to be highly sensitive to, for example, oxidative stress.[28] We are not aware of any reports characterizing the mechanisms of cell death involved in IR-induced cell death in the proliferative regions of the developing brain. In the present study, we found early signs of both p53 activation and generation of free radicals, as expected.[22] Downstream of these events, activation of both

caspase-dependent and caspase-independent mechanisms, concurrent with DNA damage and loss of proliferating (Ki-67-positive) cells, occurred. These data indicate that multiple injurious mechanisms were activated after IR, constituting possible targets for intervention.

Epo has been demonstrated to be antiapoptotic in other models of neuronal injury both *in vitro*[38] and *in vivo*.[39,40] Using a well-characterized model of neonatal hypoxia–ischemia (HI),[41,42] we observed that Epo reduced the infarct volumes by approximately 50% (unpublished observations; manuscript under revision). In this study, we were unable to detect any reduction in the loss of SVZ, GCL or myelination after IR. The lack of an effect of Epo in the IR model indicates that the injury mechanisms may be different after IR and after HI. Also, after IR cell death is observed mainly in the SVZ and SGZ, whereas after HI injury is most pronounced in differentiated, postmitotic neurons; so cell death occurs in different cellular populations to a large extent. It is possible that the IR dose used here was too high to allow Epo-mediated protection. On the other hand, we did not observe any protection by Epo in the contralateral hemisphere either, where the IR dose and injury are expected to be milder (Figure 9).

XIAP is the most potent and versatile member of the IAP family,[25] and recent studies have demonstrated that overexpression of XIAP in the mouse brain results in neuroprotection in models of focal ischemia in adult animals[43] and HI in P10 mice.[44] A transient increase in XIAP also rendered human carcinoma cells resistant to γ-IR.[45] Using the TG-XIAP mice overexpressing the protein in neurons,[43] we studied the role of caspases in apoptotic, IR-induced injury to neuronal progenitors in the SGZ of the DG. As expected, activation of the initiator caspase-9 and executor caspase-3 was significantly reduced, as judged by the immunoreactivity for the active forms of these proteases at 6 h post-IR. At this time point, apoptotic and other markers of injury peaked in this model of IR-induced injury. However, decreased caspase activation did not result in rescue of hippocampal neurons; the reduction in GCL size was the same for WT and TG-XIAP mice 7 days post-IR. In addition to the caspase-dependent mechanisms, caspase-independent mechanisms, including nuclear translocation of AIF, are activated during apoptosis.[46] Genetic inactivation of AIF rendered embryonic stem cells resistant to cell death after serum deprivation and, furthermore, AIF-induced cell death displayed structural signs of apoptosis and could be genetically uncoupled from APAF-1 and caspase-9.[47] We observed increased nuclear translocation of AIF in irradiated TG-XIAP mice compared with WT animals. Translocation of AIF has been shown to correlate well with induction of cell death after hypoglycemia,[48] brain trauma[49] and after neonatal[24] as well as adult[23,50] ischemia. Seizure-induced, newborn neurons in the DG die, at least partly, through caspase-dependent mechanisms.[51] Increased translocation of AIF may explain why overexpression of XIAP could not rescue the tissue, despite decreased caspase activation and protective effects demonstrated in the same strain of mice in models of adult focal ischemia[43] and neonatal HI.[44] We hypothesize that the cells shift from caspase-dependent to caspase-independent mechanisms of cell death, for example, mediated by AIF. The exact mechanisms, however, underlying this shift and its functional consequences for assessment of cell death after IR, remain to be identified.

In summary, we have set up and characterized a rodent model to assess the effects of ionizing radiation on brain damage. We also explored two antiapoptotic treatment strategies to counteract cell death in the developing brain. Neither treatment with Epo nor inhibition of caspases by means of transgenic overexpression of XIAP could mitigate the injury observed after IR. In the TG-XIAP mice, we observed a shift from caspase-dependent to caspase-independent mechanisms of cell death in the DG that may compensate for decreased caspase activation. Taken together, the results indicate that additional treatment strategies need to be considered in alleviating the detrimental effects observed after IR to the developing brain and in children with malignant brain tumors.

Materials and Methods

Animals

All animal experimental protocols were approved by the Ethical Committee of Göteborg (203-2001 and 184-2003). Wistar rats were from B&K Universal, Solna, Sweden. Transgenic XIAP-overexpressing (TG-XIAP) mice were produced as described.[43] The Thy 1 promoter used to drive the neuronal XIAP expression was active postnatally. WT mice were from the same source as the ones used to produce the TG-XIAP animals (Charles River, Sulzfeld, Germany).

Irradiation procedure

For IR, a linear accelerator (Varian Clinac 600CD) with 4 MV nominal photon energy and a dose rate of 2.3 Gy/min was used. Wistar rats (8-day-old) or C57/BL6 mice (10-day-old) of both sexes were anesthetized with an intraperitoneal injection of tribromoethanol (Sigma, Stockholm, Sweden), placed in a prone position (head to gantry) on an expanded polystyrene bed. The left cerebral hemisphere of each animal was irradiated with an asymmetrical radiation field of 1×2 cm with no divergence toward the right hemisphere. The source to skin distance was approximately 99.5 cm. The head was covered with a 1 cm tissue equivalent. In each case, a single absorbed dose of 4, 8 or 12 Gy was administered. The dose variation within the target volume was estimated to be $\pm 5\%$. The entire procedure was completed within 10 min. After IR, the pups were returned to their biological dams until killed. The sham control animals were anesthetized but not subjected to IR.

Tissue preparation

Animals were deeply anesthetized 2, 6, 12, 24 h or 7 days after IR, and transcardially perfusion-fixed with 4% paraformaldehyde in 0.1 M phosphate-buffered saline (PBS). The brains were removed and immersion-fixed in the same solution at 4°C for 24 h, dehydrated with a graded series of ethanol and xylene, embedded in paraffin and cut into 5 μm coronal sections.

Histological and immunohistochemical procedures

Sections were stained with thionin/acid fuchsin for morphological analysis, and adjacent sections were immunostained using the following primary

antibodies and working concentrations: rabbit anti-nitrotyrosine as a marker of oxidative stress (1 : 200 in PBS with 0.2% Triton X-100; A-21285, Molecular Probes, Eugene, OR, USA), rabbit anti-p53 (1 : 100 diluted with PBS; sc-6243, Santa Cruz Biotechnology, Santa Cruz, CA, USA), mouse anti-Ki-67 antigen as a marker of proliferating cells (1 : 25 in PBS; clone MIB-5, M 7248, DAKO, Glostrup, Denmark), rabbit anti-active caspase-3 (1 : 50 in TBS-T (Tris-buffered saline with 0.1% Tween 20); 67342A, Pharmingen, San Diego, CA, USA), goat anti-AIF (1 : 50 in TBS-T; sc-9416, Santa Cruz Biotechnology), mouse anti-MBP (1 : 10 000; SMI 94, Sternberger Monoclonals, Lutherville, MD, USA). After deparaffinization and rehydration, antigen retrieval was performed by heating the sections for 10 min in 10 mM citrate buffer (pH 6.0). Nonspecific binding was blocked with 4% horse or goat serum (depending on the species used to raise the secondary antibody) in PBS. After blocking, sections were incubated at room temperature for 1 h with primary antibodies, followed by the appropriate biotinylated secondary antibodies for 1 h (Vector Laboratories, Burlingame, CA, USA). Endogenous peroxidase activity was blocked with 0.3% H_2O_2 in methanol for 10 min, and visualization was performed using an avidin–biotin–peroxidase solution (Vectastain ABC Elite kit, Vector Laboratories). Stainings were developed with 3, 3-diaminobenzidine.

DNA fragmentation

Detection of DNA strand breaks by TUNEL was performed according to the instructions of the manufacturer (Roche Diagnostics GmbH, Mannheim, Germany). Following deparaffinization and antigen retrieval, sections were incubated with 3% bovine serum albumin in 0.1 M Tris-HCl (pH 7.5) for 30 min, followed by TUNEL reaction mixture (terminal deoxynucleotidyl transferase, fluorescein-dUTP and deoxynucleotide triphosphate) for 60 min at 37°C. Endogenous peroxidase activity was blocked with 0.3% H_2O_2 in methanol for 10 min, followed by 3% bovine serum albumin in 0.1 M Tris-HCl (pH 7.5) for 30 min at room temperature. Incubation with peroxidase-conjugated anti-fluorescein (diluted 1 : 5) at 37°C for 30 min was followed by visualization using 3,3′-diaminobenzidine.

Neuropathological analysis

Cell counting

Immunopositive and TUNEL-labeled cells were counted throughout the SVZ and the GCL, including the SGZ in the DG of the hippocampus. Three animals at each time point were examined. The numbers of positive cells were expressed as mean $\pm$ S.D.

Assessment of injury

Quantitative morphological analysis of the proliferative areas in the irradiated brains was performed on sections stained with thionin/acid fuchsin. The areas of the SVZ and the GCL (including the SGZ) in the ipsi- and contralateral hemispheres were traced and measured in three sections per animal, 10 sections (50 μm) apart, using Micro Image 4.0 (Olympus Optical Corporation). The average value obtained for each area was used as $n = 1$. The IOD of the MBP staining, taking into account both the area and intensity of the immunopositive areas, was calculated using Micro Image. IOD analysis determines the integrated amount of light passing through a material, using the following standard light transmission formula: $\mathrm{IOD} = -\log\{(\mathrm{Intensity}(x,y) - \mathrm{Black})/(\mathrm{Incident} - \mathrm{Black})\}$, where Intensity($x$,$y$) is the intensity at pixel(x,y), Black is the intensity generated when no light goes through the material and Incident is the intensity of the incident light. Before capturing images, the microscope lamp was turned on and left on for at least 15 min to yield a stable illumination. The exposure time of the CCD camera was adjusted automatically for the first image, using ViewFinder Lite (Version 1.0.125, Pixera Corporation, Los Gatos, CA, USA), and then the settings were fixed until all images had been captured. Images were captured at low-power magnification ($\times 20$ magnification) and converted to monochrome images using Studio Lite (Version 1.0.124, Pixera Corporation). Calibration of the black level in Micro Image was performed by analyzing an image that was acquired while the microscope's light pathway was shut, and calibration of incident light was performed by analyzing an image acquired when there was nothing between the microscope's lens and the light source. MBP immunostaining was examined in both hemispheres in the corpus callosum and striatum, and three sections from each animal were examined at intervals of 50 μm. The average value for each area was used as $n = 1$.

Erythropoietin treatment

Animals were treated with a single intraperitoneal dose of recombinant human Epo (Dragon Pharmaceuticals, Vancouver, Canada) or vehicle 4 h prior to IR (8 Gy). Epo was diluted to 1 U/μl in PBS with 0.1% human serum albumin and the dose was 10 U/g body weight (80 ng/g body weight). The injection volume was approximately 100–150 μl, depending on the body weight. This regime was neuroprotective in a model of neonatal HI (authors' unpublished observations). Animals were killed 7 days after IR and neuropathological analysis was performed as described above.

Statistical analysis

All values are expressed as mean $\pm$ S.D. ANOVA with Fischer's PLSD *post hoc* test was used to compare different IR doses with controls. Student's unpaired *t*-test was used to compare values between the ipsi- and contralateral hemispheres subjected to the same dose of IR, and $P < 0.05$ was considered statistically significant.

Acknowledgements

This work was supported by the Swedish Child Cancer Foundation (Barncancerfonden) (to DL, IM and KB), Jubileumsklinikens fond (to TBE), the Swedish Cancer Foundation (Cancerfonden) (to DL), the Swedish Research Council (to KB), the Frimurare Barnhus Foundation, the Göteborg Medical Society, the Åhlén Foundation, the Swedish Society of Medicine, the Wilhelm and Martina Lundgren Foundation, the Sven Jerring Foundation and the Magnus Bergvall Foundation.

References

1. Hammond GD (1986) The cure of childhood cancers. Cancer 58 (2 Suppl): 407
2. Lannering B, Marky I, Lundberg A and Olsson E. (1990) Long-term sequelae after pediatric brain tumors: their effect on disability and quality of life. Med. Pediatr. Oncol. 18: 304
3. Lannering B, Marky I and Nordborg C (1990) Brain tumors in childhood and adolescence in west Sweden 1970–1984. Epidemiology and survival. Cancer 66: 604
4. Lannering B, Rosberg S, Marky I, Moell C and Albertsson-Wikland K (1995) Reduced growth hormone secretion with maintained periodicity following cranial irradiation in children with acute lymphoblastic leukaemia. Clin. Endocrinol. (Oxford) 42: 153

5. Livesey EA and Brook CG (1988) Gonadal dysfunction after treatment of intracranial tumours. Arch. Dis. Child. 63: 495–500
6. Hall P, Adami HO, Trichopoulos D, Pedersen NL, Lagiou P, Ekbom A, Ingvar M, Lundell M and Granath F (2004) Effect of low doses of ionising radiation in infancy on cognitive function in adulthood: Swedish population based cohort study. BMJ 328: 19
7. Schultheiss TE, Kun LE, Ang KK and Stephens LC (1995) Radiation response of the central nervous system. Int. J. Radiat. Oncol. Biol. Phys. 31: 1093–1112
8. Chin HW and Maruyama Y (1984) Age at treatment and long-term performance results in medulloblastoma. Cancer 53: 1952
9. Duffner PK, Cohen ME, Thomas PR and Lansky SB (1985) The long-term effects of cranial irradiation on the central nervous system. Cancer 56 (7 Suppl): 1841
10. Li FP, Winston KR and Gimbrere K (1984) Follow-up of children with brain tumors. Cancer 54: 135
11. Packer RJ, Meadows AT, Rorke LB, Goldwein JL and D'Angio G (1987) Long-term sequelae of cancer treatment on the central nervous system in childhood 15: 241
12. Duffner PK, Cohen ME, Voorhess ML, MacGillivray MH, Brecher ML, Panahon A and Gilani BB (1985) Long-term effects of cranial irradiation on endocrine function in children with brain tumors. A prospective study. Cancer 56: 2189
13. Oberfield SE, Allen JC, Pollack J, New MI and Levine LS (1986) Long-term endocrine sequelae after treatment of medulloblastoma: prospective study of growth and thyroid function. J. Pediatr. 108: 219–223
14. Lannering B, Marky I, Mellander L and Albertsson-Wikland K (1988) Growth hormone secretion and response to growth hormone therapy after treatment for brain tumour. Acta Paediatr. Scand. Suppl. 343: 146
15. Kempermann G, Kuhn HG and Gage FH (1997) More hippocampal neurons in adult mice living in an enriched environment. Nature 386: 493–495
16. Gould E, Beylin A, Tanapat P, Reeves A and Shors TJ (1999) Learning enhances adult neurogenesis in the hippocampal formation. Nat. Neurosci. 2: 260–265
17. Shors TJ, Miesegaes G, Beylin A, Zhao M, Rydel T and Gould E (2001) Neurogenesis in the adult is involved in the formation of trace memories. Nature 410: 372–376
18. Parent JM, Tada E, Fike JR and Lowenstein DH (1999) Inhibition of dentate granule cell neurogenesis with brain irradiation does not prevent seizure-induced mossy fiber synaptic reorganization in the rat. J. Neurosci. 19: 4508–4519
19. Monje ML, Mizumatsu S, Fike JR and Palmer TD (2002) Irradiation induces neural precursor-cell dysfunction. Nat. Med. 8: 955–962
20. Hodges H, Katzung N, Sowinski P, Hopewell JW, Wilkinson JH, Bywaters T and Rezvani M (1998) Late behavioural and neuropathological effects of local brain irradiation in the rat. Behav. Brain Res. 91: 99–114
21. Sienkiewicz ZJ, Haylock RG and Saunders RD (1994) Prenatal irradiation and spatial memory in mice: investigation of dose–response relationship. Int. J. Radiat. Biol. 65: 611–618
22. Gudkov AV and Komarova EA (2003) The role of p53 in determining sensitivity to radiotherapy. Nat. Rev. Cancer 3: 117–129
23. Plesnila N, Zhu C, Culmsee C, Gröger M, Moskowitz MA and Blomgren K (2004) Nuclear translocation of apoptosis-inducing factor (AIF) after focal cerebral ischemia. J. Cereb. Blood Flow Metab. 24: 458–466
24. Zhu C, Qiu L, Wang X, Hallin U, Cande C, Kroemer G, Hagberg H and Blomgren K (2003) Involvement of apoptosis-inducing factor in neuronal death after hypoxia–ischemia in the neonatal rat brain. J. Neurochem. 86: 306–317
25. Holcik M, Gibson H and Korneluk RG (2001) XIAP: apoptotic brake and promising therapeutic target. Apoptosis 6: 253–261
26. Reddick WE, White HA, Glass JO, Wheeler GC, Thompson SJ, Gajjar A, Leigh L and Mulhern RK (2003) Developmental model relating white matter volume to neurocognitive deficits in pediatric brain tumor survivors. Cancer 97: 2512–2519
27. Fowler JF (1989) The linear–quadratic formula and progress in fractionated radiotherapy. Br. J. Radiol. 62: 679–694
28. Back SA, Gan X, Li Y, Rosenberg PA and Volpe JJ (1998) Maturation-dependent vulnerability of oligodendrocytes to oxidative stress-induced death caused by glutathione depletion. J. Neurosci. 18: 6241–6253
29. Mosier Jr. HD, Good CB, Jansons RA, Sondhaus CA, Dearden LC, Alpizar SM and Zuniga OF (1983) The effect of neonatal head-irradiation and subsequent fasting on the mechanisms of catch-up growth. Growth 47: 13–25
30. Mosier Jr. HD and Jansons RA (1970) Effect of x-irradiation of selected areas of the head of the newborn rat on growth. Radiat. Res. 43: 92–104
31. Amano T, Inamura T, Wu CM, Kura S, Nakamizo A, Inoha S, Miyazono M and Ikezaki K (2002) Effects of single low dose irradiation on subventricular zone cells in juvenile rat brain. Neurol. Res. 24: 809–816
32. Tada E, Parent JM, Lowenstein DH and Fike JR (2000) X-irradiation causes a prolonged reduction in cell proliferation in the dentate gyrus of adult rats. Neuroscience 99: 33–41
33. Peissner W, Kocher M, Treuer H and Gillardon F (1999) Ionizing radiation-induced apoptosis of proliferating stem cells in the dentate gyrus of the adult rat hippocampus. Brain Res. Mol. Brain Res. 71: 61–68
34. Parent JM, Vexler ZS, Gong C, Derugin N and Ferriero DM (2002) Rat forebrain neurogenesis and striatal neuron replacement after focal stroke. Ann. Neurol. 52: 802–813
35. Monje ML, Toda H and Palmer TD (2003) Inflammatory blockade restores adult hippocampal neurogenesis. Science 302: 1760–1765
36. Mizumatsu S, Monje ML, Morhardt DR, Rola R, Palmer TD and Fike JR (2003) Extreme sensitivity of adult neurogenesis to low doses of X-irradiation. Cancer Res. 63: 4021–4027
37. Krinke G (2000) The Laboratory Rat. (San Diego, CA: Academic Press)
38. Digicaylioglu M and Lipton SA (2001) Erythropoietin-mediated neuroprotection involves cross-talk between Jak2 and NF-kappaB signalling cascades. Nature 412: 641–647
39. Siren AL, Fratelli M, Brines M, Goemans C, Casagrande S, Lewczuk P, Keenan S, Gleiter C, Pasquali C, Capobianco A, Mennini T, Heumann R, Cerami A, Ehrenreich H and Ghezzi P (2001) Erythropoietin prevents neuronal apoptosis after cerebral ischemia and metabolic stress. Proc. Natl. Acad. Sci. USA 98: 4044–4049
40. Erbayraktar S, Grasso G, Sfacteria A, Xie QW, Coleman T, Kreilgaard M, Torup L, Sager T, Erbayraktar Z, Gokmen N, Yilmaz O, Ghezzi P, Villa P, Fratelli M, Casagrande S, Leist M, Helboe L, Gerwein J, Christensen S, Geist MA, Pedersen LO, Cerami-Hand C, Wuerth JP, Cerami A and Brines M (2003) Asialoerythropoietin is a nonerythropoietic cytokine with broad neuroprotective activity *in vivo*. Proc. Natl. Acad. Sci. USA 100: 6741–6746
41. Rice JE, Vannucci RC and Brierley JB (1981) The influence of immaturity on hypoxic–ischemic brain damage in the rat. Ann. Neurol. 9: 131–141
42. Blomgren K, Zhu C, Wang X, Karlsson JO, Leverin AL, Bahr BA, Mallard C and Hagberg H (2001) Synergistic activation of caspase-3 by m-calpain after neonatal hypoxia–ischemia: a mechanism of 'pathological apoptosis'? J. Biol. Chem. 276: 10191–10198
43. Trapp T, Korhonen L, Besselmann M, Martinez R, Mercer EA and Lindholm D (2003) Transgenic mice overexpressing XIAP in neurons show better outcome after transient cerebral ischemia. Mol. Cell. Neurosci. 23: 302–313
44. Wang X, Zhu C, Wang X, Hagberg H, Korhonen L, Sandberg M, Lindholm D and Blomgren K (2004) X-linked inhibitor of apoptosis protein (XIAP) protects against pathological caspase activation and tissue loss after neonatal hypoxia–ischemia. Neurobiol. Dis. (in press)
45. Holcik M, Yeh C, Korneluk RG and Chow T (2000) Translational upregulation of X-linked inhibitor of apoptosis (XIAP) increases resistance to radiation induced cell death. Oncogene 19: 4174
46. Susin SA, Lorenzo HK, Zamzami N, Marzo I, Snow BE, Brothers GM, Mangion J, Jacotot E, Costantini P, Loeffler M, Larochette N, Goodlett DR, Aebersold R, Siderovski DP, Penninger JM and Kroemer G (1999) Molecular characterization of mitochondrial apoptosis-inducing factor. Nature 397: 441–446
47. Joza N, Susin SA, Daugas E, Stanford WL, Cho SK, Li CY, Sasaki T, Elia AJ, Cheng HY, Ravagnan L, Ferri KF, Zamzami N, Wakeham A, Hakem R, Yoshida H, Kong YY, Mak TW, Zuniga-Pflucker JC, Kroemer G and Penninger JM (2001) Essential role of the mitochondrial apoptosis-inducing factor in programmed cell death. Nature 410: 549–554
48. Ferrand-Drake M, Zhu C, Gido G, Hansen AJ, Karlsson JO, Bahr BA, Zamzami N, Kroemer G, Chan PH, Wieloch T and Blomgren K (2003) Cyclosporin A prevents calpain activation despite increased intracellular calcium concentrations, as well as translocation of apoptosis-inducing factor, cytochrome *c* and caspase-3 activation in neurons exposed to transient hypoglycemia. J. Neurochem. 85: 1431–1442
49. Zhang X, Chen J, Graham SH, Du L, Kochanek PM, Draviam R, Guo F, Nathaniel PD, Szabo C, Watkins SC and Clark RS (2002) Intranuclear

localization of apoptosis-inducing factor (AIF) and large scale DNA fragmentation after traumatic brain injury in rats and in neuronal cultures exposed to peroxynitrite. J. Neurochem. 82: 181–191
50. Cao G, Clark RS, Pei W, Yin W, Zhang F, Sun FY, Graham SH and Chen J (2003) Translocation of apoptosis-inducing factor in vulnerable neurons after transient cerebral ischemia and in neuronal cultures after oxygen–glucose deprivation. J. Cereb. Blood Flow Metab. 23: 1137–1150
51. Ekdahl CT, Mohapel P, Weber E, Bahr B, Blomgren K and Lindvall O (2002) Caspase-mediated death of newly formed neurons in the adult rat dentate gyrus following status epilepticus. Eur. J. Neurosci. 16: 1463–1471